Tetrahedron: *Asymmetry* 24 (2013) 1303–1311

Contents lists available at ScienceDirect

Tetrahedron: *Asymmetry*

journal homepage: www.elsevier.com/locate/tetasy

Stereostructure and thermodynamic stability of atropisomers of *ortho*-substituted 2,2′-diaryl-1,1′-binaphthalenes

Marcel Ehn [a], Nikolay Georgiev Vassilev [b], Peter Kasák [a,†], Branislav Horváth [c], Juraj Filo [a], Kurt Mereiter [d], Erik Rakovský [e], Martin Putala [a,*]

[a] Department of Organic Chemistry, Faculty of Natural Sciences, Comenius University in Bratislava, Mlynská dolina, 842 15 Bratislava, Slovak Republic
[b] Institute of Organic Chemistry with Centre of Phytochemistry, Bulgarian Academy of Sciences, Acad. G. Bonchev Street, Bl. 9, 1113 Sofia, Bulgaria
[c] Chemistry Institute, Faculty of Natural Sciences, Comenius University in Bratislava, Mlynská dolina, 842 15 Bratislava, Slovak Republic
[d] Institute of Chemical Technologies and Analytics, Vienna University of Technology, Getreidemarkt 9/163, A-1060 Vienna, Austria
[e] Department of Inorganic Chemistry, Faculty of Natural Sciences, Comenius University in Bratislava, Mlynská dolina, 842 15 Bratislava, Slovak Republic

ARTICLE INFO

Article history:
Received 16 July 2013
Accepted 5 September 2013

ABSTRACT

A series of *ortho*-substituted 2,2′-aryl-1,1′-binaphthalenes were prepared via Negishi arylation of 2,2′-diiodo-1,1′-binaphthalene in good to high yields (65–95%) as an equilibrium mixtures of up to three atropisomers (*unlike,unlike*, *like,unlike*, and *like,like*). Thermodynamic stability parameters of the atropisomers were evaluated from VT NMR spectra by regression analysis. The DFT parameters calculated using CAM-B3LYP functional comprising solvent permittivity were, apart from the toluene solution, which was expected to interact with the aromatic solute, in qualitative agreement with the experimental values. In the case of the ditolyl derivative, the population of the atropisomers was confirmed by CD spectroscopy via comparison with the population-weighted averaged spectrum computed using the M06 functional. X-ray structure analyses of particular atropisomers of the dianisyl, dianilinyl, and dinaphthyl derivatives are also presented and discussed.

1. Introduction

Rotary dynamics at a molecular level have attracted continuing attention with the aim of designing artificial synthetic machines imitating the mechanical movement of macroscopic machines and machine parts.[1] Atropisomeric molecular triads of B-A-B type in which A is a (hetero)arene and B is a non symmetrical group attached to A via a bond with restricted rotation,[2] represent one of the most investigated systems with respect to their stereodynamics.[2–6] There are only few reports on B-A-B triads in which central unit A is chiral: including binaphthalene-based bissulfonamide **1**[5] and biphenyl-based dicarboxamides **2**[6] (Fig. 1). While the former can be interconverted among three diastereomeric atropisomers by rotation around the C(naphthalene)–N bonds, the latter are formed as a single diastereomer as controlled by side chain stereogenic centers.

We have developed a synthetic methodology for the efficient introduction of aryl groups at the 2- and 2′-positions of 1,1′-binaphthalene.[7] We decided to use it for the preparation of diarylbinaphthalene series **3** as triads B-A-B with a configurationally stable axially chiral central unit A and to study their stereodynamics. For this purpose, we chose hindered *ortho*-substituted phenyls as aryl groups, with increasing steric hindrance of the attached *ortho*-substituent[8] (methoxy, dimethylamino, methyl, isopropyl, and benzo).

2. Results and discussion

2.1. Synthesis and spectral properties

A series of sterically hindered diarylbinaphthalenes **3** were prepared in good to high yields (65–95%) via Negishi coupling of the corresponding arylzinc bromides with racemic as well as enantiopure (*R*)- or (*S*)-diiodide **4** (Scheme 1). An excess of arylzinc reagent was applied to ensure good yields in the case of more hindered aryl groups.

Samples of diaryl derivatives **3** for advanced study were additionally purified by preparative thin layer chromatography and/or crystallization. The measurement of their variable temperature NMR spectra revealed the presence of up to three diastereomeric atropisomers (Scheme 2): two *anti*-isomers (marked as *u*,*u* and *l*,*l*) and one *syn*-isomer (pseudo-*meso*-form, marked as *l*,*u*). Such stereochemistry originates from the configurationally stable stereogenic axis between the two naphthalene rings of the binaphthalene moiety[9] and the partially restricted rotation around the two

* Corresponding author. Tel.: +421 2 60296323; fax: +421 2 60296337.
E-mail address: putala@fns.uniba.sk (M. Putala).
† Current address: Center for Advanced Materials, Qatar University, PO Box 2713 Doha, Qatar.

0957-4166/$ - see front matter © 2013 Elsevier Ltd. All rights reserved.
http://dx.doi.org/10.1016/j.tetasy.2013.09.005

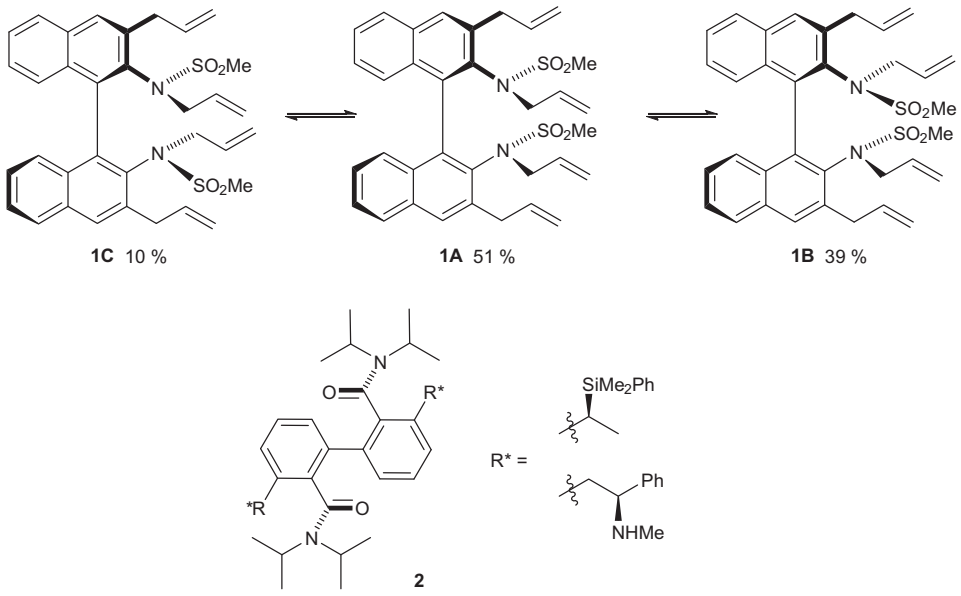

Figure 1. Examples of B-A-B triads in which the central unit A is chiral.

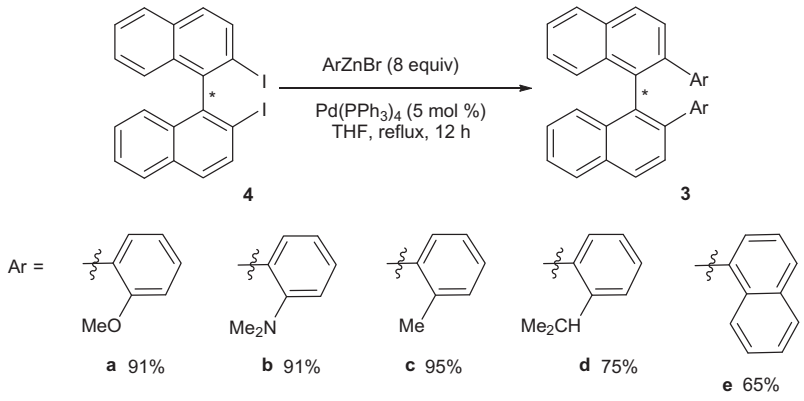

Scheme 1. Preparation of diarylbinaphthalenes **3** by Negishi arylation of diiodide **4**. The in situ preparation of arylzinc bromides from anisole, 2-bromo-*N*,*N*-dimethylaniline, 2-iodotoluene, 1-iodo-2-isopropylbenzene, or 1-bromonaphthalene: Reagents and conditions: (i) *n*-BuLi (1.2 equiv), THF, −78 to 0 °C, 2 h; (ii) $ZnBr_2$ (1 equiv), THF, −78 °C to rt, 1 h.

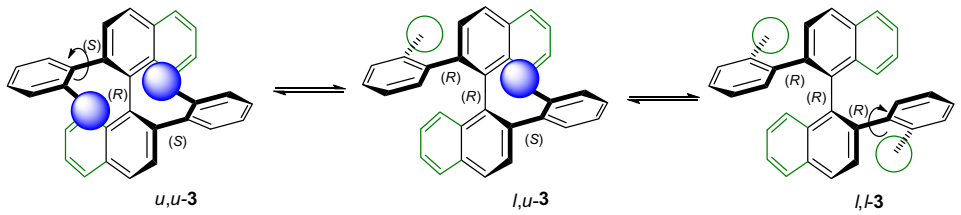

Scheme 2. Three atropisomers of diarylbinaphthalenes **3** [shown for the (*R*)-enantiomer of the binaphthalene moiety] and their interconversions.

additional stereogenic axes at each of the naphthalene-aryl connections.

Dianisyl and dianilinyl derivatives **3a** and **3b** exhibited four signals for the methyl group protons in their ^{1}H NMR spectra at lower temperatures: one signal for each of *u*,*u*- and *l*,*l*-isomers and two signals for *u*,*l*-isomer (one for each of its methyl groups). In the case of ditolyl derivative **3c**, only three signals for the methyl group protons were observed due to the absence of the minor *l*,*l*-atropisomer. As expected, bis(isopropylphenyl) derivative **3d** exhibited four signals for the methine protons of the isopropyl group, but the methyl groups of each isopropyl were found to be diastereotopic and, therefore, appearing as eight doublets. In the case of the dinaphthyl derivative **3e**, the signals of the major *u*,*u*-diastereomer were only observed in ^{1}H and ^{13}C NMR spectra, as assigned by further X-ray structure analysis (see Section 2.3).

Assignments of the methyl group signals in the ^{1}H NMR spectra to particular atropisomers were based on predictions using DFT calculations[10] in the GAUSSIAN 09 program[11] with the B3LYP functional[12] in chloroform, as well as on the equal integral intensities of both of *l*,*u*-atropisomer signals (respective of all four signals in the case of **3d**). An excellent agreement between the calculated and observed chemical shifts was found for dianisyl, dianilinyl, and ditolyl compounds **3a–c** (deviations ranging from 0.01 to 0.12 ppm). A qualitative agreement was observed for

bis(isopropylphenyl) derivative **3d** (Table 1), where assignment of the isopropyl group signals was based on cross-peaks in the COSY spectrum (Fig. 2).

Enantiopure samples of compounds **3** exhibited absolute values of specific rotation ranging from 67 to 140, except for the much higher value of 888 for the dinaphthyl derivative **3e**. In all cases, positive values were found for (*R*)-at-binaphthalene derivatives **3** and negative for (*S*) ones. The configuration of the binaphthalene central unit is, therefore, decisive with regard to the sign of specific rotation seeing that different atropisomers are prevailing for particular derivatives **3** (see Table 2).

The CD spectrum of ditolyl derivative (*S*)-**3c** was examined in order to verify the contribution of individual atropisomers.[13] Figure 3 shows the CD spectra of all three atropisomers of **3c** together with their population-weighted average (taking experimentally determined values of population given in Table 2), calculated

Table 1
^{1}H NMR chemical shifts (δ, ppm) of methyl group protons of compounds **3** atropisomers in chloroform: calculated at the B3LYP/6-311G(d,p) level/assigned in experimental spectra

Compound	*l*,*l*	*l* of *l*,*u*	*u* of *l*,*u*	*u*,*u*
3a	2.62/2.51	2.69/2.70	3.41/3.51	3.31/3.37
3b	1.46/1.45	1.74/1.70	1.82/1.90	1.89/2.01
3c	1.28/not observed	1.60 *l*, 1.59 *u*/1.61, 1.57		1.22/1.27
3d	1.20, 0.43/ 1.23, 0.25	1.38, 0.62/ 1.01, 0.45	1.78, 1.34/ 1.38, 1.10	1.33, 0.96/ 0.74, −0.04

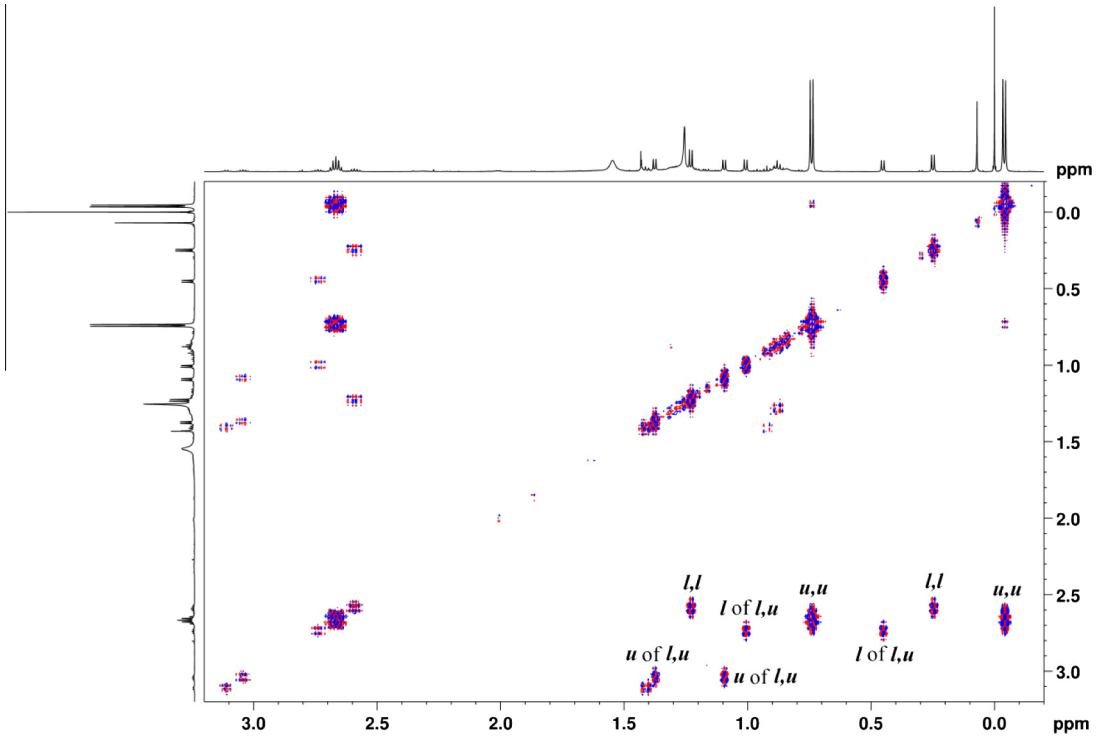

Figure 2. ^{1}H COSY NMR spectrum (600 MHz, $CDCl_3$) of bis(isopropylphenyl) derivative **3d** for signals of isopropyl groups with their assignment to atropisomers.

Table 2
Comparison of theoretical and experimental thermodynamic parameters for compound **3** atropisomers at 298 K

Comp.	Atropisomer	Solvent	Theoretical values[a]				Experimental values[b]			
			ΔH (kJ/mol)	ΔS (J/Kmol)	ΔG (kJ/mol)	Population (%)	ΔH (kJ/mol)	ΔS (J/Kmol)	ΔG (kJ/mol)	Population (%)
3a	*u*,*u*	Dichloromethane	0.00	0.00	0.00	40.1	0.00	0.00	0.00	19.2
	l,*u*		2.77	10.01	−0.22	43.8	4.11(13)	23.37(58)	−2.85(2)	60.8
	l,*l*		5.37	10.43	2.26	16.1	9.14(2)	31.02(88)	−0.10(3)	20.0
3b	*u*,*u*	Toluene	0.00	0.00	0.00	81.6	0.00	0.00	0.00	25.3
	l,*u*		4.37	1.36	3.97	16.5	6.03(19)	14.55(76)	1.70(4)	12.8
	l,*l*		4.66	−14.93	9.11	1.9	4.59(19)	22.85(78)	−2.22(4)	61.9
3c	*u*,*u*	Dichloromethane	0.00	0.00	0.00	98.8	0.00	0.00	0.00	91.7
	l,*u*		9.94	−3.43	10.96	1.2	9.38(24)	11.46(82)	5.96(4)	8.3
	l,*l*		20.27	−1.63	20.76	0.02	Not observed			
3d	*u*,*u*	Chloroform	0.00	0.00	0.00	91.7	0.00	0.00	0.00	68.1
	l,*u*		8.22	4.74	6.81	5.9	2.37(6)	−2.79(23)	3.20(2)	18.7
	l,*l*		7.27	−5.75	8.98	2.4	−1.57(7)	13.39(23)	4.08(2)	13.1
3e	*u*,*u*	Chloroform	0.00	0.00	0.00	80.1	0.00	0.00	0.00	>96
	l,*u*		5.01	5.12	3.48	19.6	Not observed			
	l,*l*		16.47	7.87	14.12	0.27	Not observed			

[a] Calculated by the DFT method at CAM-B3LYP/6-31G(d) level.
[b] Evaluated by regression analysis from experimental ^{1}H NMR data. Quoted errors are the statistical errors based on scattering of the data points around Van't Hoff straight line only. The absolute error in temperature is assumed to be not more than 0.1 K.

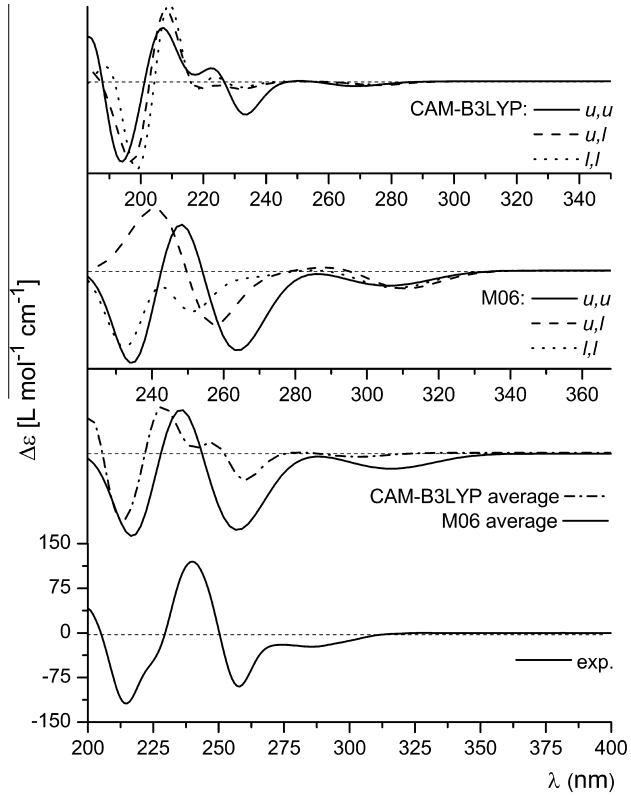

Figure 3. CD spectra of the three atropisomers of (*S*)-**3c** calculated using M06 and CAM-B3LYP functionals with the 6-31G(d) basis set (*u,u* solid line, *u,l* dashed line, *l,l* dotted line) and comparison of the weight-averaged calculated spectra (using the experimentally determined ratio of atropisomers given in Table 2 with the experimental CD spectrum in hexane–dimethoxyethane (99:1).

by CAM-B3LYP[14] and M06,[15] and compared to the experimental CD spectrum. An excellent agreement can be observed for the population-weighted averaged spectrum computed using the M06 functional, while the results of the CAM-B3LYP calculations are

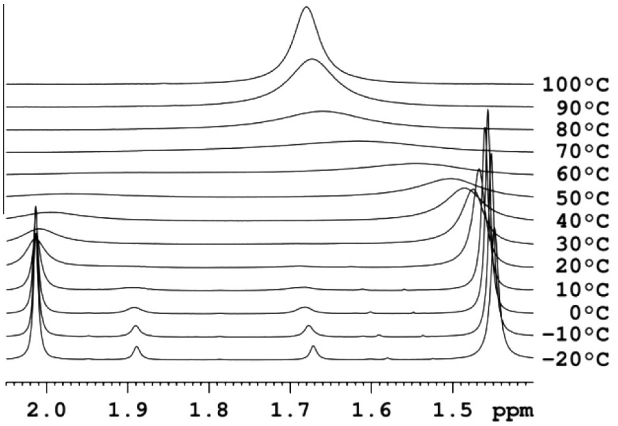

Figure 4. ^{1}H VT NMR spectra (600 MHz, toluene-d_8) of dianisyl derivative **3b**, part for signals of dimethylamino group protons.

inferior but still in a good agreement. In order to describe the spectroscopic pattern of the experimental CD spectrum in the given spectroscopic region, it was necessary to employ more electronic transitions when CAM-B3LYP was used.

2.2. Thermodynamic stability of the atropisomers

Derivatives **3a–c** with a smaller group attached at phenyl's *ortho*-position showed a broadening of the signals for the methyl group protons in the ^{1}H NMR spectra upon heating up to their coalescence (as shown for **3b** in Fig. 4), while this behavior was not observed in the spectra of derivatives **3d** and **3e** bellow 100 °C. The tendency for the acceleration of atropisomerization upon heating follows the expected order of increasing atropisomerization barriers with increasing steric effect of the attached groups:[8] methoxy **3a** < dimethylamino **3b** < methyl **3c** < isopropyl **3d** ~ benzo **3e**. However, the determination of the atropisomerization barriers for such complex systems is not trivial and will be a subject of further studies in our laboratory.

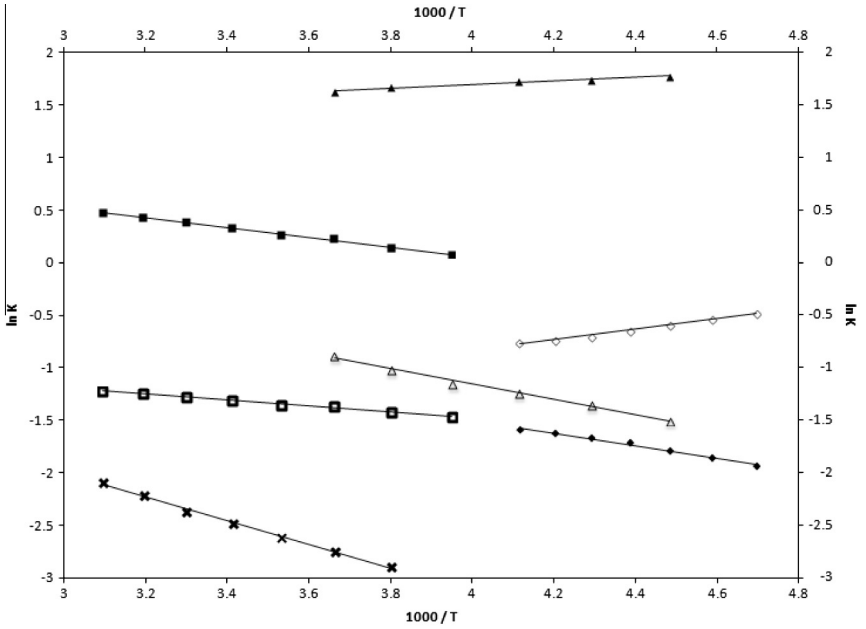

Figure 5. Plots of equilibrium constants *K* against reciprocal absolute temperature *T* for atropisomerizations: (◇) *u,u*-**3a** to *l,u*-**3a**, (♦) *l,u*-**3a** to *l,l*-**3a**, (△) *u,u*-**3b** to *l,*u-**3b**, (▲) *l,u*-**3b** to *l,l*-**3b**, (×) *u,u*-**3c** to *l,u*-**3c**, (□) *u,u*-**3d** to *l,u*-**3d**, (■) *l,u*-**3d** to *l,l*-**3d**.

Integration of the signals for the methyl group protons in the ^{1}H NMR spectra of compounds **3a–d** measured at different temperatures (from the temperature range with sharp signals) allowed us to determine the temperature dependent populations of the individual atropisomers.[16] The data were evaluated by regression analysis with very good R^2 values, varying from 0.961 to 0.99 (Fig. 5). Based on the analysis, experimental relative thermodynamic stability parameters (ΔG, ΔH and ΔS) were calculated for individual atropisomers and populations of atropisomers at room temperature were estimated or more precisely determined (Table 2).

Experimentally determined thermodynamic parameters were compared with those calculated by DFT methods at the CAM-B3LYP/6-31G(d) level including solvent permittivity (Table 2). Good qualitative agreement was found for the relative stability of atropisomers for ditolyl, bis(isopropylphenyl), and dinaphthyl derivatives **3c–e**. In the case of dianisyl derivative **3a**, the correct major *l*,*u*-atropisomer was predicted by theoretical calculations. The disagreement between the theory and experiment in the case of dianilinyl derivative **3b** (observed also at the higher level of theory) is most probably due to the specific interaction with the solvent molecules (toluene), which would have to be taken into account as individual molecules and not just as environment permittivity.

2.3. X-ray structure analysis

In the crystal structure of (*R*)-**3a** (Fig. 6), the asymmetric unit consists of one half of the (*R*,*R*,*R*)-2,2′-bis(2-methoxyphenyl)-1,1′-binaphthalene molecule (*l*,*l*-atropisomer) lying on a twofold rotation axis thus adopting a C_2 symmetry. Since this atropisomer is not the major one in solution (Table 2), spontaneous dynamic resolution had to occur during crystallization. The intermolecular contacts between molecules are based on a weak C17–H...O interaction with d(C...O) = 3.178 Å and (apparent) C–H...O angle of 124°. These bonds form infinite supramolecular chains with graph set descriptor C(4).[17] The crystal structure determination revealed that the solid state compound is a solvate of the type host–guest compound, that is, in a chiral stable framework of (*R*,*R*,*R*)-**3a**, molecules are infinite spiral-like channels at 0,0,z which contain a disordered petroleum ether. The amount of solvent could be estimated from four to six CH_2 groups per **3a** molecule.

In the crystal structure of (*R*)-**3b** (Fig. 7), the asymmetric unit contains one molecule of (*R*,*R*,*R*)-2,2′-bis[2-(dimethylamino) phenyl]-1,1′-binaphthalene (*l*,*l*-atropisomer) with C_1 symmetry. This atropisomer is also the major one in solution (Table 2). The intermolecular contacts are based on C–H...π interactions C14B–H14B...C6B^a/C7B^a, where superscript ^{a} represents symmetry operation ($3/2 - x$, $1 - y$, $-1/2 + z$).

The asymmetric unit of (*RS*)-**3e** (Fig. 8) consists of one half of the *u*,*u*-atropisomer of (*R*)- or (*S*)-1,2′:1′,1″:2″,1‴-quaternaphthalene molecules, lying on a twofold rotation axis, thus having C_2 symmetry. The compound crystallizes in the *C*2/*c* space group as a racemate. Interactions in the structure are mainly based on C–H...π interactions C4–H4A...C18^b/C19^b, where superscript ^{b} denotes symmetry operation ($1/2 - x$, $1/2 - y$, $1 - z$), and π–π interactions, which are given in Table 3. As a result of the intermolecular π–π interactions, the molecules are in the layers parallel to the (100) plane.

Table 4 shows the effect of closed packing and intermolecular interactions in a solid state structure on dihedral angles (between naphthyl planes of binaphthalene and between naphthyl and attached aryl planes) by comparison of the values calculated at B3LYP/6-31G(d) level for individual molecules in vacuo to those found in the solid state structures. The largest difference between these values among the studied compounds was observed for dianisyl derivative **3b**. The observed difference is most probably caused by orientation of the dimethylamino group in the solid state to the center of its molecule minimizing the electrostatic repulsion between the nitrogen lone pairs of neighboring molecules (Fig. 7).

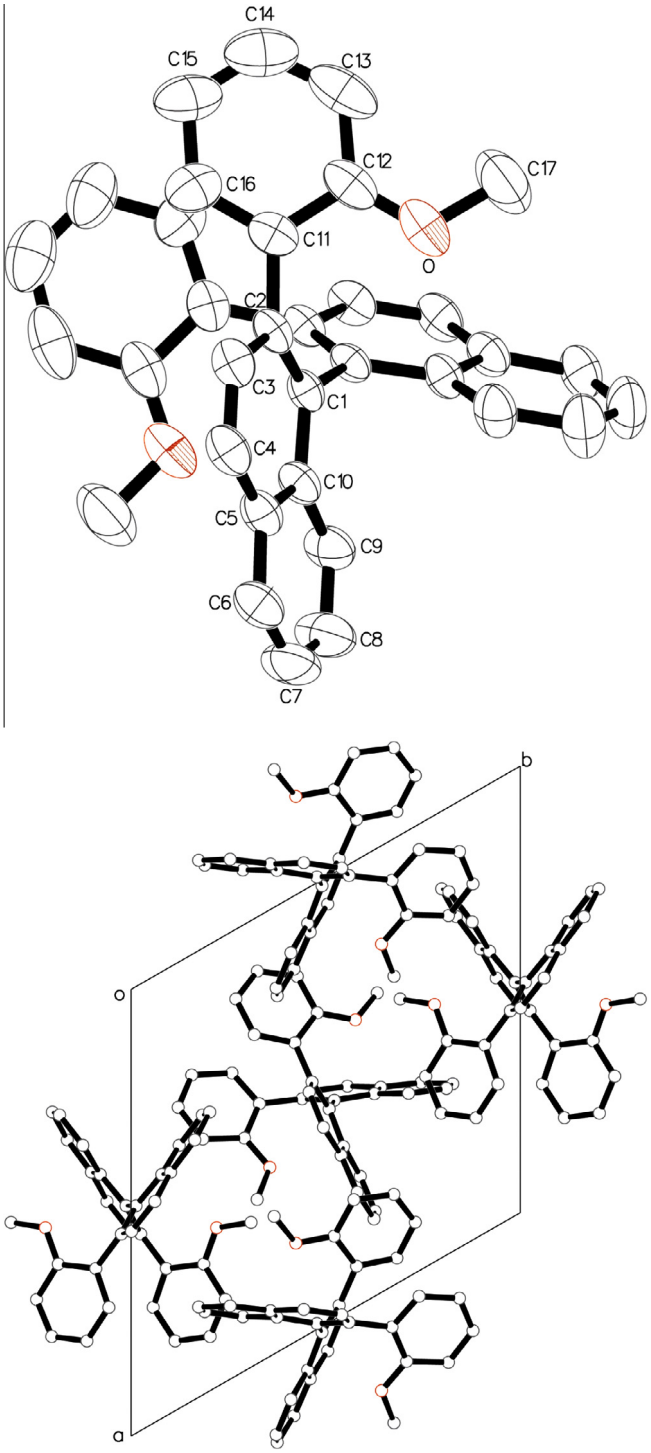

Figure 6. Top: crystal structure of compound (*R*)-**3a** with numbering scheme. All non-hydrogen atoms are drawn as 50% probability ellipsoids; H atoms are omitted for clarity. The symmetry operation relating labeled atoms to unlabeled atoms is (y, x, $1 - z$). Bottom: view of the compound (*R*)-**3a** cell packing along the *c* axis.

3. Conclusion

In conclusion we have prepared a series of *ortho*-substituted 2,2′-aryl-1,1′-binaphthalenes **3** exhibiting atropisomerization by

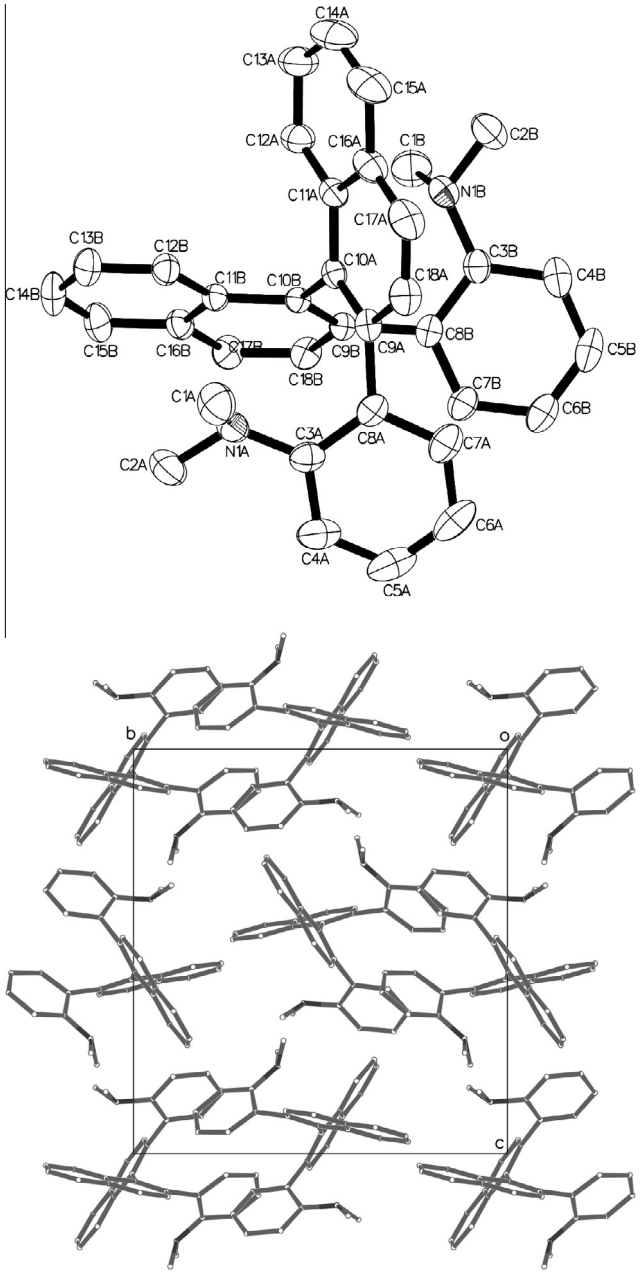

Figure 7. Top: crystal structure of compound (*R*)-**3b** with numbering scheme. All non-hydrogen atoms are drawn as 30% probability ellipsoids; H atoms are omitted for clarity. Bottom: view of the compound (*R*)-**3b** cell packing along the *a* axis.

rotation around the C(naphthyl)–C(aryl) bonds. ^{1}H NMR signals of the methyl group protons for individual atropisomers were reliably assigned according to the calculated chemical shifts (DTF B3LYP). Thermodynamic stability parameters of the atropisomers were evaluated from VT NMR spectra by regression analysis and were

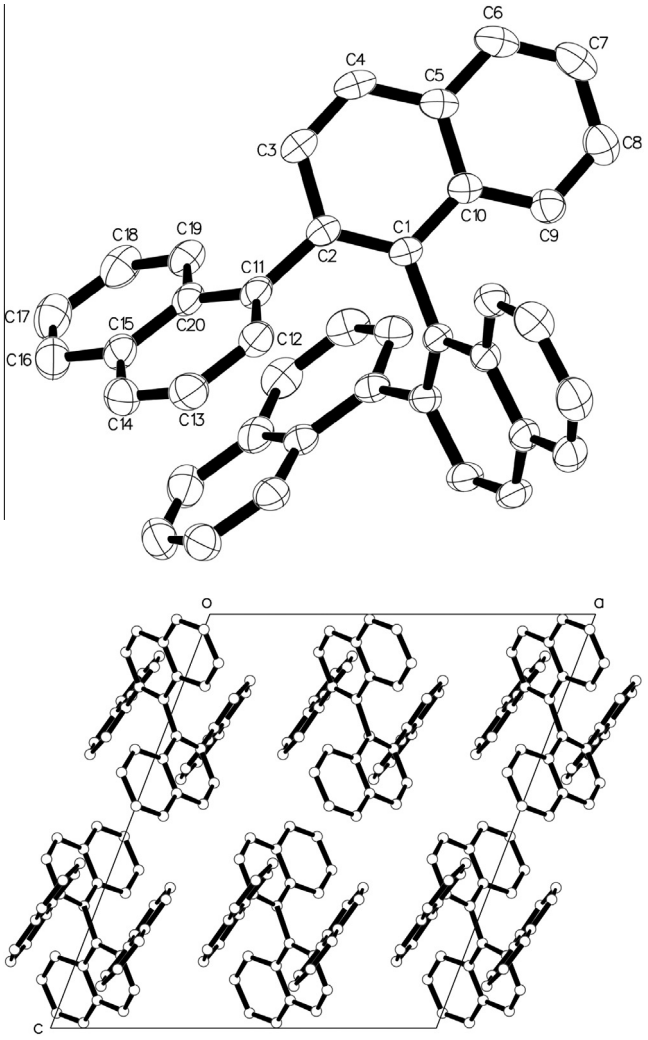

Figure 8. Top: (*S*)-**3e** molecule from crystal structure of compound (*RS*)-**3e** with numbering scheme. All non-hydrogen atoms are drawn as 50% probability ellipsoids; H atoms are omitted for clarity. The symmetry operation relating labeled atoms to unlabeled atoms is $(-x, y, 1/2 - z)$. Bottom: view of the compound (*RS*)-**3e** cell packing along the *b* axis.

Table 4
Comparison of calculated and found dihedral angles in molecular structures of compounds **3**

Compound atropisomer	Dihedral angle	6-31G(d)	X-ray
(*R*,*R*,*R*)-**3a**	Np-Np′: C2-C1-C1′-C2′	−74.2°	−71.1 (3)°
	Np-Ar: C1-C2-C11-C12	−68.4°	−60.6 (3)°
(*R*,*R*,*R*)-**3b**	Np-Np′: C9A-C10A-C10B-C9B	−84.2°	−70.4 (2)°
	Np-Ar: C10A-C9A-C8A-C3A	−52.9°	−60.0 (2)°
	Np′-Ar′: C10B-9B-C8B-C3B	−52.9°	−65.2 (2)°
(*S*,*R*,*R*)-**3e**	Np-Np′: C2-C1-C1′-C2′	81.0°	77.1 (1)°
	Np-Ar: C1-C2-C11-C20	−123.4°	−118.8 (1)°

Table 3
π–π Interactions in the crystal structure of (*RS*)-**3e**

Ring 1	Ring 2	Angle	Centroid–centroid distance (Å)	Shift distance (Å)
C11-C12-C13-C14-C15-C20	C15-C16-C17-C18-C19-C20[a]	9.80°	3.97	1.77
C5-C6-C7-C8-C9-C10	C5-C6-C7-C8-C9-C10[b]	0°	3.93	1.96
C15-C16-C17-C18-C19-C20	C15-C16-C17-C18-C19-C20[a]	8.72°	3.57	0.54

[a] Intramolecular interaction with symmetry operation $(-x, y, ½ - z)$.
[b] Intermolecular interaction with symmetry operation $(-x, 1 - y, 1 - z)$.

found to be in good qualitative agreement with the calculated values except for ditolyl derivative **3c** which is expected to interact with aromatic solvent. The population of the ditolyl derivative **3c** atropisomers was confirmed by CD spectroscopy in comparison with the population-weighted averaged spectrum computed using the M06 functional. The X-ray structure analyses of the dianisyl **3a**, dianilinyl **3b**, and dinaphthyl **3e** derivatives revealed the presence of a single atropisomer in the solid state structure with intramolecular C–H...O for **3a**, C–H...π for **3b**, and **3e** and π–π interactions for **3e**. The solid state molecular structure of dianisyl derivative **3b** differed from the calculated geometry due to intramolecular nitrogen lone electron pair repulsion.

4. Experimental

4.1. General

All moisture and air-sensitive reactions were carried out under an inert atmosphere. Solvents were dried and purified by standard methods before use. Column chromatography was performed on Merck silica gel 60, thin-layer chromatography was performed on Merck TLC—plates silica gel 60, F-254. Preparative thin-layer chromatography was performed on Merck PLC plates—silica gel 60, F-254, 2 mm (20 × 20). Melting points were determined with a Melting Point M-656 Bűchi apparatus and are uncorrected. Specific rotations were measured on a JASCO P-2000 Polarimeter and are given in deg cm^{-3} g^{-1} dm^{-1}. ECD spectra were recorded on a Jasco J815 instrument. NMR spectra were recorded on Varian Mercury Plus Instrument (300 MHz for ^1H, 75 MHz for ^{13}C), Varian NMR System 600 (600 MHz for ^1H and 150.8 MHz for ^{13}C NMR), and Bruker Avance II+ 600 MHz spectrometer using BBO probehead (600 MHz for ^1H NMR) at 25 °C if not given otherwise. The temperature was calibrated before the VT experiments by means of a thermocouple, which has an uncertainty not exceeding 0.1 °C. Chemical shifts are reported in δ ppm referenced to an internal $SiMe_4$ standard for ^1H NMR. The following abbreviations are used: s = singlet, d = doublet, t = triplet, sept = septet, m = multiplet, br = broad. The mass spectra were obtained by ultrafleXtreme mass spectrometer (MALDI TOF/TOF, Bruker) using 2,5-dihydroxybenzoic acid as matrix and PEG 600 sodium adducts as calibrant. Compounds (*R*)-, (*S*)- and (*RS*)-2,2′-diiodo-1,1′-binaphthalene **4** were prepared from 2,2′-diamino-1,1′-binaphthalene according to the published procedure.[4]

4.2. Preparation of 2,2′-diaryl-1,1′-binaphthalenes 3

A round-bottom double necked flask fitted with a reflux condenser was charged with substituted benzene or aryl halide (6.3 mmol, 8 equiv): anisole (0.68 g), 2-bromo-*N*,*N*-dimethylaniline (1.26 g), 1-iodotoluene (1.38 g), 1-iodo-2-isopropylbenzene (1.56 g) or 2-bromonaphthalene (1.31 g), THF (12.6 mL, 1 M solution of aryl halide) under an inert atmosphere. Next, it was cooled to −78 °C and a solution of *n*-BuLi (1.6 M in hexanes, 4 mL, 6,3 mmol, 8 equiv) was added dropwise. Then it was allowed to warm up to 0 °C and stirred for 2 h at this temperature, after which $ZnBr_2$ (1,4 g, 6,3 mmol, 8 equiv) was added as a 1.5 M solution in THF. After stirring for 1 h, the resulting mixture was allowed to warm up to room temperature. A solution of 2,2′-diiodo-1,1′-binaphthalene **4** (400 mg, 0.79 mmol, 1 equiv) and $Pd(PPh_4)$ (54.8 mg, 0.047 mmol, 6 mol %) dissolved in dry THF (4 mL) was then added dropwise. The reaction mixture was then refluxed overnight. The reaction was then quenched with aqueous 1 M HCl (4 mL). The organic layer was separated and the water layer was extracted 3 times with Et_2O (5 mL). The combined organic layers were dried over Na_2SO_4 and concentrated under reduced pressure. The product was then purified by multiple column chromatography and/or preparative thin layer chromatography over silica gel.

4.2.1. (*R*)-2,2′-Bis(2-methoxyphenyl)-1,1′-binaphthalene 3a

Eluent hexanes/ethyl acetate = 4/1; yield 336 mg (91%); single crystals were obtained by crystallization from mixture of toluene/petroleum ether; mp 167–169 °C; $[\alpha]_D^{20} = +139.9$(*c* 0.51, CH_2Cl_2); ^1H NMR (300 MHz, $CDCl_3$): δ = 7.87 (d, *J* = 8.08 Hz, 2H), 7.81 (d, *J* = 8.49 Hz, 2H), 7.44–7.22 (m, 8H), 7.06–7.00 (m, 2H), 6.49 (br s, 4H), 6.27 (br s, 2H) 2.82 (br s, 6H, OCH_3). ^{13}C NMR (75 MHz, $CDCl_3$) δ 151.15, 131.02, 130.22, 129.26, 127.13, 126.31, 124.55, 123.46, 122.64, 121.81, 120.35, 119.91, 115.18, 114.22, 105.92, 104.16, 48.63.

4.2.2. (*R*)-2,2′-Bis[2-(dimethylamino)phenyl]-1,1′-binaphthalene 3b

Eluent hexanes/$CHCl_3$/Et_3N = 96/3/1.2; yield 354 mg (91%); single crystals were obtained by crystallization from hexane; mp 209–211 °C with decomposition; $[\alpha]_D^{20} = +66.7$ (*c* 0.53, CH_2Cl_2); ^1H NMR (300 MHz, $CDCl_3$): δ = 7.90–7.81 (m), 7.41–7.36 (m), 7.26–7.15 (m), 7.04–6.99 (m), 6.91–6.86 (m), 6.71 (m), 6.49 (d, *J* = 7.9 Hz), 6.26–6.22 (m), 6.03 (d, *J* = 7.2 Hz), 2.01 (s, *u*,*u*-$N(CH_3)_2$), 1.90 (s, *u* of *l*,*u*-$N(CH_3)_2$), 1.73 (s, *l* of *l*,*u*-$N(CH_3)_2$), 1.48 (s, *l*,*l*-$N(CH_3)_2$).^{13}C NMR (75 MHz, $CDCl_3$): δ = 151.65, 138.70, 136.25, 135.39, 134.90, 134.14, 132.15, 129.91, 129.52, 127.97, 127.76, 127.22, 124.72, 124.54, 122.51, 117.11, 42.46.

4.2.3. (*S*)-2,2′-Bis(2-methylphenyl)-1,1′-binaphthalene 3c

Eluent hexanes/CH_2Cl_2 = 49/1; yield 326 mg (95%); mp 206–208 °C; $[\alpha]_D^{20} = -76.5$ (*c* 0.5, CH_2Cl_2); ^1H NMR (600 MHz, $CDCl_3$): δ = 7.91 (d, *J* = 8.1 Hz, 2H), 7.82 (d, *J* = 8.5 Hz, 2H), 7.47 (m, 2H), 7.31–7.29 (m, 2H), 7.27–7.25 (m, 4H), 7.03 (m, 2H), 6.96–6.92 (m, 2H), 6.60–6.54 (m, 4H), 1.61 (s, *l*,*u*-CH_3), 1.57 (s, *l*,*u*-CH_3), 1.27 (s, *u*,*u*-CH_3) ^{13}C NMR (75 MHz, $CDCl_3$) δ 140.74, 138.41, 136.55, 135.38, 134.58, 132.24, 130.69, 129.54, 129.51, 128.21, 127.80, 127.01, 126.78, 126.56, 125.64, 124.71, 19.91 (CH_3); HRMS (MALDI, *m*/*z*) calcd for $C_{34}H_{26}$ 434.2035, found 434.2025.

4.2.4. (*R*)-2,2′-Bis(2-isopropylphenyl)-1,1′-binaphthalene 3d

Eluent hexanes/CH_2Cl_2 = 49/1, hexanes; yield 291 mg (75%); mp 124–130; $[\alpha]_D^{20} = +74.6$ (*c* 0.93, CH_2Cl_2); ^1H NMR (300 MHz, $CDCl_3$): δ = 8.00–7.80 (m), 7.58–7.28 (m), 7.23–6.92 (m), 6.82–6.77 (m), 6.60–6.53 (m), 6.29–6.14 (m), 3.04 (sept, *J* = 6.8, Hz, *u* of *l*,*u*-$CHMe_2$) 2.78–2.55 (m, *u*,*u*-, *l*,*l*- and *l* of *l*,*u*;-$CHMe_2$); 1.38 (d, *J* = 6.6 Hz, *u* of *l*,*u*-CH_3), 1.23 (d, *J* = 6.8 Hz, *l*,*l*-CH_3), 1.10 (d, *J* = 6.7 Hz, *u* of *l*,*u*-CH_3), 1.01 (d, *J* = 6.8 Hz, *l* of *l*,*u*-CH_3), 0.74 (d, *J* = 6.8 Hz, *u*,*u*-CH_3), 0.45 (d, *J* = 6.8 Hz, *l* of *l*,*u*-CH_3), 0.25 (d, *J* = 6.8 Hz, *l*,*l*- CH_3), -0.04 (d, *J* = 6.8 Hz, *u*,*u*-CH_3); including signals of (*R*,*S*,*S*)-**1d** (*u*,*u*-atropisomer): 7.86 (d, *J* = 7.9, 2H), 7.84 (d, *J* = 8.5, 2H), 7.40 (ddd, *J* = 8.1, 7.9, 1.1 Hz 2H), 7.34 (d, *J* = 8.2 Hz 2H), 7.27 (d, overlapped with solvent, 2H), 7.20 (ddd, *J* = 8.3, 8.2, 1.3, 2H), 7.08 (ddd, *J* = 7.8, 7.6, 1.2 Hz, 2H), 6.93 (dd, *J* = 7.9, 1.1 Hz, 2H), 6.79 (ddd, *J* = 7.5, 7.5, 1.3, 2H), 6.16 (dd, *J* = 7.7, 1.3 Hz, 2H), 2.67 (sept, *J* = 6.8 Hz, $CHMe_2$), 0.74 (d, *J* = 6.8 Hz, CH_3), −0.04 (d, *J* = 6.8 Hz, CH_3); ^{13}C NMR (75 MHz, $CDCl_3$): major signals δ = 146.81, 140.04, 140.02, 133.85, 133.31, 132.66, 132.20, 130.70, 128.08, 127.87, 127.65, 126.74, 125.76, 125.23, 125.02, 124.19, 29.70, 29.55, 29.24, 25.51, 21.16. HRMS (MALDI, *m*/*z*) calcd for $C_{38}H_{34}$ 490.2661, found 490.2689.

4.2.5. (*R*,*S*,*S*)-1,2′:1′,1″:2″,1‴-Quaternaphthalene 3e

Eluent hexanes/CH_2Cl_2 = 49/1; yield 260 mg (65%); single crystals were obtained by crystallization of *rac*-**3e** from toluene; mp 194–196 °C; $[\alpha]_D^{20} = +888.3$ (*c* 1.06, CH_2Cl_2); ^1H NMR (300 MHz, $CDCl_3$): δ = 7.98 (d, *J* = 8.1 Hz, 2H), 7.84 (d, *J* = 8.5 Hz, 2H), 7.55

(ddd, J = 8.1, 8.0, 1.4 Hz, 2H), 7.48–7.28 (m, 10H), 6.92–6.85 (m, 4H), 6.81 (dd, J = 7.1, 1.4 Hz, H), 6.36 (ddd, J = 8.5, 8.2, 1.2 Hz, 2H), 6.09 (d, J = 8.5 Hz, 2H). ^{13}C NMR (75 MHz, $CDCl_3$): δ = 138.50, 137.70, 135.74, 135.57, 133.77, 132.42, 131.99, 130.56, 128.37, 128.01, 127.26, 127.12, 126.84, 126.72, 126.49, 125.89, 125.12, 125.09, 125.04, 124.23.

4.3. X-ray structure determination

Intensity data for **3a** and **3e** were collected on a Bruker Smart APEX CCD three-circle diffractometer using graphite-monochromated MoKα radiation (0.71073 Å) at 173 K. Data collection and cell refinement were done by Bruker SMART software (AXS Inc., Madison, Wisconsin, USA, 2003), data reduction and correction for Lorentz and polarization effects were carried by Bruker SAINT software. Multi-scan absorption correction (SADABS) was used.

Intensity data for **3b** were collected on a Kuma KM-4 CCD κ-axis diffractometer using graphite-monochromated MoKα radiation (0.71073 Å) at room temperature (293 K). The diffraction intensities were corrected for Lorentz and polarization effects. Absorption correction was based on a Gaussian integration with beam profile correction. Data collection, cell refinement, data reduction, and finalization including all corrections mentioned above were carried by CrysAlis Pro software (CrysAlis Pro, 1.171.36.28, Agilent Technologies UK Ltd., Oxford, UK, 2013.).

The structures were solved by SHELXS-97 using direct methods and refined by SHELXL-97 (with exception of **3b**, where SHELXL-2013 package was used) using the full-matrix least squares method on all F^2 data.[18] All non-H atoms were refined anisotropically as free atoms; H atoms were placed geometrically using riding constraints and refined with U_{iso} = 1.2 $U_{eq}(C_{sp}{}^2)$ or 1.5 $U_{eq}(C_{sp}{}^3)$, respectively. CH_3 groups were oriented toward electron density maxima. The absolute configurations of all compounds mentioned were known from the synthesis. In the case of **3a**, the crystals are a solvate of petroleum ether with the solvent disordered in continuous spiral-shaped channels along the c-axis at about 0, 0, z. The solvent accessible void volume is 325.0 Å^3 per unit cell. The electron count of the solvent calculated by PLATON[19] is 22 e$^-$ per cell. The most prominent solvent peaks were at (x, y, z): (−0.007793, 0.098869, 0.279207), (−0.083854, −0.020759, 0.224310), and (−0.008554, 0.092215, 0.196392). The solvent was squeezed with program PLATON and is not contained in chemical formula and quantities derived thereof.

Geometrical analysis was performed using SHELXL and PLATON. OLEX2 was used for structure drawings.[20] Crystal data and conditions of data collection and refinement are reported in Table 5.

4.4. Calculations

Calculations were carried out with the GAUSSIAN 09 software[8] at the DFT level of theory. Final optimization of the atropisomer geometries for compounds **3** was accomplished using B3LYP[9] functional with 6-31G(d) basis set.[21] The ΔH, ΔS, and ΔG values were calculated for T = 293.15 K at the same level of theory including zero-point energy in the particular solvent environment (represented by relative permittivity) and vibrational, rotational, and translational thermal energy corrections. The ^{1}H NMR chemical shifts in a particular solvent environment were calculated using B3LYP functional[12] with 6-311G(d,p) basis set.[22] ECD spectra of **3c** atropisomers were calculated using CAM-B3LYP[14] and M06[15] functionals with 6-31G(d) basis set.[21]

4.5. Crystal data

CCDC 950187-950189 contain the supplementary crystallographic data for compounds **3b**, **3e**, and **3a**. These data can be obtained free of charge via http://www.ccdc.cam.ac.uk/conts/retrieving.html, or from the Cambridge Crystallographic Data Centre, 12 Union Road, Cambridge CB2 1EZ, UK; fax: +44 1223 336 033; or e-mail: deposit@ccdc.cam.ac.uk. ^{1}H, ^{13}C NMR spectra of compounds **3**, VT NMR of **3a**, **3c**, and **3d**, HRMS analyses of **3c** and 3d are available.

Table 5
X-ray crystallographic experimental data for compounds **3a**, **3b**, and **3e**

Empirical formula	$C_{34}H_{26}O_2$ **3a**	$C_{36}H_{32}N_2$ **3b**	$C_{40}H_{26}$ **3e**
M_r	466.55	492.63	506.61
Crystal system, space group	Trigonal, $P3_121$	Orthorhombic, $P2_12_12_1$	Monoclinic, C2/c
Unit cell dimensions	Determined from 6444 reflections	Determined from 18150 reflections	Determined from 6002 reflections
a [Å], α [°]	14.9293(3), 90	11.78263(17), 90	14.7084(8), 90
b [Å], β [°]	14.9293(3), 90	14.7055(2), 90	11.2004(6), 110.9100(10)
c [Å], γ [°]	10.7844(5), 120	16.0166(2), 90	17.0143(9), 90
V [Å^3]	2081.64(11)	2775.17(7)	2618.3(2)
Z, Z'	3, 1	4, 1	4, 1
μ [mm^{-1}], ρ (calcd) [g cm^{-3}]	0.068, 1.117	0.068, 1.179	0.073, 1.285
F(000)	738	1048	1064
Absorption correction, T_{min}, T_{max}	Multi-scan, 0.90, 0.99	GAUSSIAN, 0.77, 2.03	Multi-scan, 0.89, 1.00
Extinction correction	None	SHELXL, 0.0089(11)	SHELXL, 0.0039(7)
Crystal size [mm]	0.52 × 0.22 × 0.20	1.01 × 0.98 × 0.60	0.55 × 0.52 × 0.33
Crystal habit, color	Prism, colorless	Block, colorless	Prism, colorless
θ Range for data collection [°]	2.46–28.26	3.27–27.85	2.35–27.00
Limiting indices	h = −19 → 19	h = −15 → 15	h = −18 → 15
	k = −19 → 19	k = −19 → 19	k = −13 → 14
	l = −14 → 14	l = −20 → 20	l = −21 → 21
Reflections collected/unique/observed [$I > 2\sigma(I)$]	20834/3425/2946 [R_{int} = 0.0423, Friedel opposites not merged]	46544/6286/5745 [R_{int} = 0.0224, Friedel opposites not merged]	9900/2854/2466 [R_{int} = 0.0230, Friedel opposites not merged]
Completeness to θ [°]	98.9% to 28.26°	99.8% to 26.37°	99.9% to 27°
Data/restraints/parameters	3425/0/163	6286/0/348	2854/0/182
Final weighting scheme	$w = 1/[\sigma^2(F_o^2) + (0.1116P)^2 + 0.1610P]$ where $P = (F_o^2 + 2F_c^2)/3$	$w = 1/[\sigma^2(F_o^2) + (0.0376P)^2 + 0.362P]$ where $P = (F_o^2 + 2F_c^2)/3$	$w = 1/[\sigma^2(F_o^2) + (0.0586P)^2 + 1.1193P]$ where $P = (F_o^2 + 2F_c^2)/3$
Absolute structure determination	From synthesis	From synthesis	—
S (goodness-of-fit)	1.065	1.053	1.062
Final R indices [$I > 2\sigma(I)$]	R = 5.87%, wR = 16.23%	R = 3.50%, wR = 8.58%	R = 3.99%, wR = 10.66%
Final R indices (all data)	R = 6.70%, wR = 17.00%	R = 4.01%, wR = 8.99%	R = 4.55%, wR = 11.29%
Largest difference peak/hole [e Å^{-3}]	0.503/−0.157	0.125/−0.105	0.276/−0.224

Acknowledgments

Authors are thankful to Professor A. Mannschreck (University of Regensburg) for initial fruitful discussions on atropisomerizations. This work was supported by the Slovak Grant Agency for Science (grant No. 1/0623/12), the Bulgarian Science Fund (Projects UNA-17/2005, RNF01/0110 and DRNF-02/13) and by COST action CM0802 'PhoSciNet'. This publication is the result of the project implementation: Center of excellence for green chemistry methods and processes supported by the Research & Development Operational Programme funded by the ERDF.

References

1. (a) Koumura, N.; Zijlstra, R. W. J.; van Delden, R. A.; Harada, N.; Feringa, B. L. *Nature* **1999**, *401*, 152–155; (b) Kelly, T. R.; De Silva, H.; Silva, R. A. *Nature* **1999**, *401*, 150–152; (c) Balzani, V.; Credi, A.; Raymo, F. M.; Stoddart, J. F. *Angew. Chem.* **2000**, *112*, 3484–3530; (d) Balzani, V.; Credi, A.; Raymo, F. M.; Stoddart, J. F. *Angew. Chem., Int. Ed.* **2000**, *39*, 3348–3391; (e) Special issue on molecular machines: *Acc. Chem. Res.* **2001**, *34*.; (f) Sauvage, J. P. *Molecular Machines and Motors*; Springer: Berlin, 2001; (g)*Molecular Motors*; Schliwa, M., Ed.; Wiley-VCH: Weinheim, 2002; (h) Balzani, V.; Credi, A. *Molecular Devices and Machines—A Journey into the Nanoworld*; Wiley-VCH: Wein-heim, 2003; (i) Leigh, D. A.; Wong, J. K. Y.; Dehez, F.; Zerbetto, F. *Nature* **2003**, *424*, 174–179; (j) Hernandez, J. V.; Kay, E. R.; Leigh, D. A. *Science* **2004**, *306*, 1532–1537; (k) Mandl, C. P.; König, B. *Angew. Chem., Int. Ed.* **2004**, *43*, 1622–1624; (l) Kelly, T. R. *Top. Curr. Chem.* **2005**, 262; (m) Kottas, G. S.; Clarke, L. I.; Horinek, D.; Michl, J. *Chem. Rev.* **2005**, *105*, 1281–1376; (n) Lehn, J.-M. *Chem. Eur. J.* **2006**, *12*, 5910–5915; (o) Browne, W. R.; Pollard, M. M.; de Lange, B.; Meetsma, A.; Feringa, B. L. *J. Am. Chem. Soc.* **2006**, *128*, 12412–12413; (p) Saha, S.; Stoddart, J. F. *Chem. Soc. Rev.* **2007**, *36*, 77–92; (q) Kay, E. R.; Leigh, D. A.; Zerbetto, F. *Angew. Chem.* **2007**, *46*, 72–191.
2. Gawronski, J.; Kacprzak, K. *Chirality* **2002**, *14*, 689–702 (and references cited therein).
3. Mazzanti, A.; Lunazzi, L.; Casarini, D. *Eur. J. Org. Chem.* **2010**, 2035–2056 (and references cited therein).
4. Recent examples: (a) Zakai, U. I.; Bzoch-Mechkour, A.; Jacobsen, N. E.; Abrell, L.; Lin, G.; Nichol, G. S.; Bally, T.; Glass, R. S. *J. Org. Chem.* **2010**, *75*, 8363–8371; (b) Chong, Y. S.; Dial, B. E.; Burns, W. G.; Shimizu, K. D. *Chem. Commun.* **2012**, 1296–1298; (c) Talele, R. H.; Sahoo, S.; Bedekar, A. V. *Org. Lett.* **2012**, *14*, 3166–3169.
5. Pluempanupat, W.; Abraham, M.; Brecker, L.; Wolschann, P.; Karpfen, A.; Arion, V. B.; Widhalm, M. *J. Org. Chem.* **2011**, *76*, 3222–3230.
6. Clayden, J.; Lund, A.; Youssef, L. H. *Org. Lett.* **2001**, *3*, 4133–4136.
7. Krascsenicsova, K.; Walla, P.; Kasák, P.; Uray, G.; Kappe, O.; Putala, M. *Chem. Commun.* **2004**, 2606–2607.
8. Schlosser, M.; Lunazzi, L.; Mancinelli, M.; Mazzanti, A.; Lepri, S.; Ruzziconi, R. *Org. Biomol. Chem.* **2012**, *10*, 1847–1855.
9. (a) Cooke, A. S.; Harris, M. M. *J. Chem. Soc.* **1963**, 2365–2373; (b) Putala, M. *Enantiomer* **1999**, *4*, 243–262.
10. Examples for ^{1}H NMR calculations at the same level of theory: (a) Micco, D. S.; Chini, G. M.; Riccio, R.; Bifulo, G. *Eur. J. Org. Chem.* **2010**, 1411–1434; (b) Dračínský, M.; Pohl, R.; Slavětínská, L.; Buděšínský, M. *Magn. Reson. Chem.* **2010**, *48*, 718–726.
11. Frisch, M. J.; Trucks, G. W.; Schlegel, H. B.; Scuseria, G. E.; Robb, M. A.; Cheeseman, J. R.; Scalmani, G.; Barone, V.; Mennucci, B.; Petersson, G. A.; Nakatsuji, H.; Caricato, M.; Li, X.; Hratchian, H. P.; Izmaylov, A. F.; Bloino, J.; Zheng, G.; Sonnenberg, J. L.; Hada, M.; Ehara, M.; Toyota, K.; Fukuda, R.; Hasegawa, J.; Ishida, M.; Nakajima, T.; Honda, Y.; Kitao, O.; Nakai, H.; Vreven, T., ; Montgomery, J. A., Jr.; Peralta, J. E.; Ogliaro, F.; Bearpark, M.; Heyd, J. J.; Brothers, E.; Kudin, K. N.; Staroverov, V. N.; Kobayashi, R.; Normand, J.; Raghavachari, K.; Rendell, A.; Burant, J. C.; Iyengar, S. S.; Tomasi, J.; Cossi, M.; Rega, N.; Millam, J. M.; Klene, M.; Knox, J. E.; Cross, J. B.; Bakken, V.; Adamo, C.; Jaramillo, J.; Gomperts, R.; Stratmann, R. E.; Yazyev, O.; Austin, A. J.; Cammi, R.; Pomelli, C.; Ochterski, J. W.; Martin, R. L.; Morokuma, K.; Zakrzewski, V. G.; Voth, G. A.; Salvador, P.; Dannenberg, J. J.; Dapprich, S.; Daniels, A. D.; Farkas, Ö.; Foresman, J. B.; Ortiz, J. V.; Cioslowski, J.; Fox, D. J. GAUSSIAN *09, Revision A.02*; Gaussian, Inc.: Wallingford CT, 2009.
12. (a) Becke, A. D. *Phys. Rev. A* **1988**, *38*, 3098–3100; (b) Becke, A. D. *J. Chem. Phys.* **1993**, *98*, 5648–5652; (c) Lee, C.; Yang, W.; Parr, R. G. *Phys. Rev. B* **1988**, *37*, 785–789.
13. Examples: (a) Julínek, O.; Setnička, V.; Miklášová, N.; Putala, M.; Ruud, K.; Urbanová, M. *J. Phys. Chem. A* **2009**, *113*, 10717–10725; (b) Uray, G.; Wagner, U. G.; Fabian, W. M. F. *Comput. Theor. Chem.* **2011**, *977*, 103–110.
14. Yanai, T.; Tew, D. P.; Handy, N. C. *Chem. Phys. Lett.* **2004**, *393*, 51–57.
15. Zhao, Y.; Truhlar, D. G. *Theor. Chem. Acc.* **2008**, *120*, 215–241.
16. Examples for the application of the van't Hoff plot from ^{1}H NMR: (a) Taha, A. N.; Neugebauer Crawford, S. M.; True, N. S. *J. Phys. Chem. A* **1998**, *102*, 1425–1430; (b) Goto, H.; Furusho, Y.; Miwa, K.; Yashima, E. *J. Am. Chem. Soc.* **2009**, *131*, 4710–4719.
17. Bernstein, J.; Davis, R. E.; Shimoni, L.; Chang, N.-L. *Angew. Chem., Int. Ed. Engl.* **1995**, *34*, 1555–1573.
18. Sheldrick, G. M. *Acta Crystallogr., Sect. A* **2008**, *64*, 112–122.
19. Spek, A. L. *J. Appl. Crystallogr.* **2003**, *36*, 7–13.
20. Dolomanov, O. V.; Bourhis, L. J.; Gildea, R. J.; Howard, J. A. K.; Puschmann, H. *J. Appl. Crystallogr.* **2009**, *42*, 339–341.
21. Hariharan, P. A.; Pople, J. A. *Theor. Chim. Acta* **1973**, *28*, 213–222.
22. (a) McLean, A. D.; Chandler, G. S. *J. Chem. Phys.* **1980**, *72*, 5639–5648; (b) Wachters, A. J. H. *J. Chem. Phys.* **1970**, *52*, 1033–1037; (c) Hay, P. J. *J. Chem. Phys.* **1977**, *66*, 4377–4384; (d) McGrath, M. P.; Radom, L. *J. Chem. Phys.* **1991**, *94*, 511–516.